Rates of Diffusion of Fluorescent Molecules via Cell-to-Cell Membrane Channels in a Developing Tissue

RICHARD G. A. SAFRANYOS and STANLEY CAVENEY
Department of Zoology, University of Western Ontario, London, Ontario N6A 5B7, Canada

ABSTRACT Diffusion coefficients for the intercellular movement of fluorescent tracers have been measured in the epidermis of a larval beetle. Fluorescent tracer was injected into a cell and the spread of tracer from cell to cell in this monolayer was recorded by a TV camera. Fluorescence intensities were digitized from the TV images at successive times after the start of injection at various distances from the source by a microcomputer interfaced with a video analyzer. From the relationship between concentration (measured as light intensity), time and distance, an effective diffusion coefficient (D_e) is calculated for the tracer in the tissue. In newly ecdysed epidermis, D_e for carboxyfluorescein (CF) is 2.7×10^{-7} cm^2/s, and D_e for lissamine rhodamine B (LRB) is 1.2×10^{-7} cm^2/s, whereas in intermolt epidermis the D_e's for CF and LRB are 3.7×10^{-7} and 1.2×10^{-7} cm^2/s, respectively. These diffusion coefficients are only an order of magnitude lower than their values in water. The ratio of D_e for the two tracers at these two stages of development differs from the ratio predicted in cytoplasm alone, with the movement of the slightly larger molecule (LRB) being impeded relative to that of the smaller molecule (CF). This suggests that the properties of the membrane channels amplify differences in the rates of movement of molecules of similar size. This may be important during cell patterning in development. D_e for CF was also monitored as junctional resistance was increased in the epidermis. During 30 min of exposure to 0.25 mM chlorpromazine, D_e dropped to 20% of its initial value of 5×10^{-7} cm^2/s, implying that the junctional membrane, rather than cytoplasm, is the major barrier to molecular diffusion among the cells.

Cell-to-cell membrane channels function in the maintenance of homeostasis among cells in a tissue, the mediation of hormonal responses, and possibly in coordinating cellular activities in developing and differentiating tissues (2, 22, 25). These channels permit the movement of ions and small molecules from the cytoplasm of one cell to that of another (24, 25). It has been proposed that these channels may also allow the diffusion of key molecules (morphogens) among cells for the establishment of gradients of positional information during development (11, 53). Recent evidence suggests that at developmental compartment boundaries the movement of larger dye molecules via these channels may be impeded but that the movement of inorganic ions is not (3, 23, 47, 50). It becomes important, therefore, to determine the precise relationship between these two levels of junctional communication and whether they may be regulated independently (by such factors as cytosolic pH [39] and Ca^{++} levels [35, 36], and transjunctional voltage [38]).

Although junctional conductance to inorganic ions has been measured in developing cells and cells in culture (reviewed in reference 25), few estimates of the diffusion rate of organic molecules among cells within tissues exist. The problem of measuring the rate of movement of molecules via these cell-to-cell channels has been approached in a number of ways. A "cut-end" approach (originally developed by Weidmann [48]) has been used to calculate the movement of K^+ (48), tetraethylammonium ions (49), cAMP (42), fluorescein (12), and procion yellow (16) through the intercalated disks of mammalian cardiac muscle and 2-deoxyglucose in mammalian myometrium (9). This technique requires large pieces of essentially homogeneous tissues, and that the cells be arranged in an almost linear fashion. Michalke (28) determined the rate of movement of [^{3}H]hypoxanthine from prelabeled to unlabeled cells in cultures of liver cells as they grew confluent.

More recently, the microinjection of fluorescent dyes has permitted the direct visualization of the movement of molecules from cell to cell. The combination of fluorescence

THE JOURNAL OF CELL BIOLOGY · VOLUME 100 MARCH 1985 736-747

microscopy with either photographic or video microscopy (4, 17, 44, 51) permits both the direct observation of the process and later quantitation of the images. Complicated geometries (usually nonhomogeneous cell volumes and shapes) have been a problem in these recent studies. Nevertheless, the movement of (*a*) sodium fluorescein in atrioventricular node cells (32), (*b*) derivatives of fluorescein in earthworm giant axons (4), (*c*) carboxyfluorescein in cultured pancreatic islet cells (18), and (*d*) lucifer yellow in Novikoff hepatoma cells (21) has been measured.

We present here effective diffusion coefficients for fluorescent molecules measured in a cell sheet by a computer–video method. The tissue used, the epidermis of the mealworm *Tenebrio molitor*, has a simple geometry (a monolayer of cells of uniform height [7]), and its cells possess gap junctions (8). In addition, the junctional conductance of the epidermal cells has been previously measured in response to a variety of treatments, including hormone application (7) exposure to Ca^{++} ionophore and cyclic nucleotides (6) and to inhibitors of calmodulin (20).

Our results show that the rate of diffusion of small cytoplasmic molecules from cell to cell is very rapid, and their movement in this tissue is about an order of magnitude slower than that in water. In addition, we show that the membrane channels connecting the cells appear to retard the movement of one of a pair of molecules of similar size.

MATERIALS AND METHODS

Cell Preparation: Penultimate (0.06–0.08 g) and ultimate (>0.12 g) instar larvae of *Tenebrio molitor* were collected immediately after ecdysis and kept at 26–27°C. Before use, animals were anesthetized and sterilized by immersion into 70% methanol for 5 min. Squares of epidermis were excised from the ventral surface of abdominal segments III–VI and placed into tissue culture medium, pH 6.7 (7), except that medium M199 (Gibco Laboratories, Grand Island, NY) was used in place of medium HB597 (Connaught Laboratories, Toronto, Ontario). All fat body and adhering muscle was removed. Preparations not used immediately were kept in an incubator at 27°C in an atmosphere containing 2% CO_2. Each preparation consisted of a monolayer of ~20,000 epidermal cells of uniform height (10 ± 1 μm in intermolt larvae [7]; 16–18 μm in newly ecdysed larvae [8]), attached to the rigid and transparent cuticle. The epidermis was clamped into a 35-mm diam petri dish containing medium, and the cells in the center of the preparation were observed with a Zeiss IM35 inverted microscope (Carl Zeiss, Inc., New York) fitted with phase-epifluorescence optics (× 40 Neofluar objective, numerical aperture 0.75). Chlorpromazine (Sigma Chemical Co., St. Louis, MO) was made up as a 0.25 mM solution in tissue culture medium.

Tracer Injection: Two fluorescent dyes, 6-carboxyfluorescein (mol wt 376; Eastman Kodak Co., Rochester, NY) and lissamine rhodamine B200 (mol wt 559; Polysciences, Inc., Warrington, PA), were used as cell-to-cell tracers. They were made up as 10 mM solutions in distilled water; the pH was adjusted to 7.0 with 1 N NaOH, and then filtered through a Millipore filter (0.2-μm pore size, Millipore Corp., Bedford, MA). Glass microelectrodes (Kwikfil capillary tubing, No. 1B100F; W-P Instruments, Inc., New Haven, CT) were pulled on a vertical microelectrode puller (Narashige Scientific Laboratory, Tokyo). Electrode tips were back-filled with dye solutions by capillary action and mounted onto deFonbrune micromanipulators (CH Beaudouin, Paris) in the electrophysiological setup described previously (7). The preparation was grounded through an Ag/AgCl electrode and a KCl/agar bridge immersed in the bathing medium. Tracer was injected into the cells by iontophoresis using a continuous train of hyperpolarizing current pulses (0.2-s duration, one per second) of 6 nA unless otherwise stated. This pulse caused a small drop in membrane potential of ~3 mV in the source cell.

Each electrode was first checked with its tip in the culture medium (at some distance from the tissue) to see that its resistance was acceptably low (between 100 and 300 MΩ) and that it delivered fluorescent puffs of tracer into the medium when the iontophoretic current was turned on. The electrode was then inserted into a cell. The current pulses aided electrode penetration greatly. The dye delivered into the medium near the injected cell diffused rapidly away and did not obscure its detection in the source cell. Because the microelectrode also recorded the membrane potential of the source cell and the moment of electrode entry, the quality of the penetration and the stability of the cell during injection could be monitored. These dye-filled electrodes had higher resistance than our conventional KCl-filled electrodes (15–40 MΩ). They recorded a lower range of apparent membrane potential (20–40 mV) because of low electrometer impedance. After several penetrations with a dye electrode, the normal range of membrane potential for a particular epidermal preparation became apparent. If the membrane potential fell during injection, that particular "spread" of tracer was rejected. A 30-s period of injection was sufficient for the calculation of diffusion coefficients.

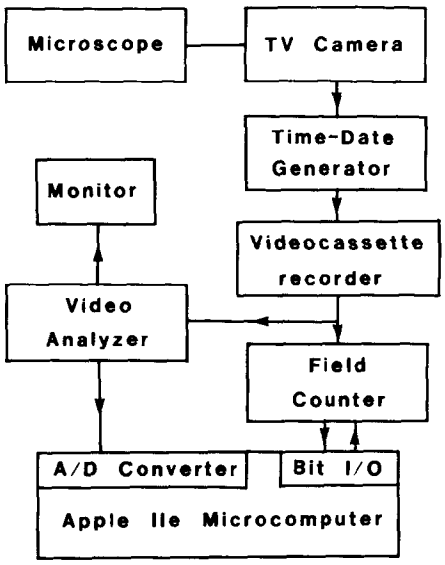

FIGURE 1 Arrangement of equipment for video recording and analysis.

Carboxyfluorescein (CF)[1] and lissamine rhodamine B (LRB) were excited by light from a mercury vapor lamp (HBO 50 W) using the following Zeiss interference-filter sets: excitation filters, BP485 (CF) and BP546 (LRB); barrier filters, BP520 (CF) and LP580 (LRB); with dichroic mirrors: FT510 (CF), and FT580 (LRB).

Video Recording and Analysis: A modified RCA silicon-intensified target (SIT) television camera (TC1030/H; RCA Electro-Optics & Devices, Lancaster, PA) was attached via a Zeiss TV connector to the cineport of the inverted microscope. Both the automatic gain control and target control of this camera provided fixed gain which could be adjusted manually. The procedure for these modifications is described in the RCA 1030H service manual (33). All quantitative fluorescence measurements were made with the automatic gain control and target control in the same fixed position. A black reference (darkest portion of the image) was set by placing a strip of black tape on the photoreticule in the intermediate-image plane (33).

Fig. 1 illustrates the arrangement of the equipment for video recording and analysis. The video signal from the camera was sent to an RCA video time-date generator (TC 1440B), and the combined signal was recorded on a Sony (TVO-9000) ¾-in time-lapse videocassette recorder. The composite video signal from the tape-recorder was coupled to a Colorado Video Analyzer 321 (Colorado Video, Inc., Boulder, CO) and the image displayed on an RCA 14-in black and white monitor (TC1214). The brightness or light intensity (in volts) along a vertical cursor that intersected each of the horizontal TV lines of a particular TV field (known as "slowscan," see Fig. 3) was digitized by an A/D converter (Mountain Hardware Inc., Scotts Valley, CA) and by appropriate software within an Apple IIe microcomputer (Apple Computer, Inc., Cupertino, CA). The field counter used vertical and horizontal synchronization from the video signal and a machine language subroutine to time correctly the sampling of the slowscan signal (13).

The epidermis was oriented on the microscope stage so that its anterior-posterior axis ran parallel to the direction of electrode entry. Tracer spreads were analyzed perpendicular to this axis. For each spread, the concentration of tracer was related to the light intensity, distance was measured in TV lines (calibrated with a micrometer slide as 1.01 μm/TV line), and time was measured by counting TV fields (60 fields/s). On playback of the tape, the vertical cursor of the video analyzer was placed across the center of the image of the dye spread. The field counter was set to sample every 60th or 120th TV field. The

[1] *Abbreviations used in this paper:* CF, carboxyfluorescein; CPZ, chlorpromazine; D_e, effective diffusion coefficient; LRB, lissamine rhodamine B; SIT, silicon-intensified target.

digital light intensities from 100 successive TV lines across the spread in a given field (sampled in real time, i.e., one sample per TV line, every 64 μs) were stored as a two-dimensional matrix in the computer. Each column in the matrix contained the light intensities from one TV field while each row in the matrix contained the changing light intensities at a given point with time.

Response Characteristics of the SIT Camera: The response of the SIT camera to light emitted from known concentrations of fluorescent tracer was determined with a microrefractometer slide (Zeiss micro-interference refractometer II). This slide, normally used to determine the refractive index with small volumes, is optically flat and has a precision-gound well (shaped as a sphere segment) at its center. The microrefractometer that we used had a well 8.32 μm deep and 205 μm wide.

A 1.0-μl droplet of dye solution was applied to the surface of the slide, near the well, with a micrometer syringe and 30-gauge needle (Roger Gilmont Instruments, Inc., Great Neck, NY). The test chamber containing the dye solution was completed by placing a 18-mm diam coverslip on top of the droplet. Provided that the slide and lower surface of the coverslip were free of dust, the droplet spread evenly to fill the space between them. The microrefractometer slide was then inverted, and excess fluid was pressed from the test chamber onto tissue paper, and the slide was placed onto the microscope stage. This procedure made a chamber in which peak fluorescence in the well was ~10 times that of the surrounding area (except at camera saturation) (Fig. 2, *inset*). Dye fluorescence in the chamber was observed and recorded on videotape with the same objective (× 40, numerical aperture 0.75) used in the experiments.

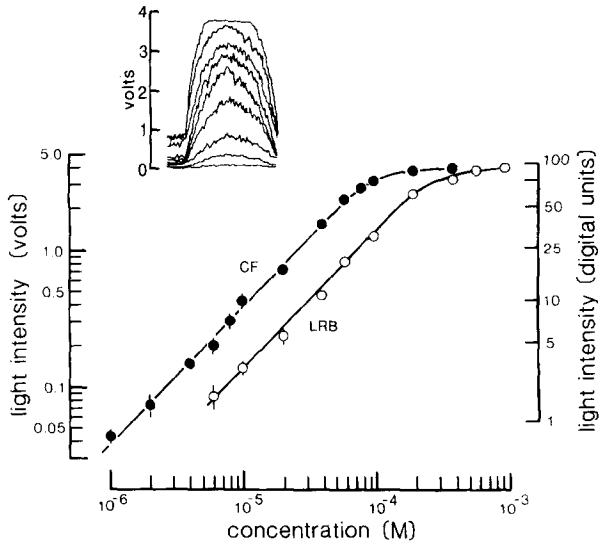

FIGURE 2 Response of the SIT camera to increasing concentrations of fluorescent dye. The dye solution was applied to the microrefractometer slide and the fluorescence within and around the well in the slide detected by the camera and recorded on videotape. During playback, the intensity profile of fluorescence during the first 0.2 s of excitation was sampled by the vertical cursor of the video analyzer along a line passing through the center of the well. The voltages associated with this transect of the video signal were displayed on an oscilloscope. Light-intensity profiles for different concentrations of CF displayed in this manner are shown in the inset. The voltages plotted in the two calibration curves were read directly from the oscilloscope screen and are the voltages (mean ± SD, n = 3–6 for each dye and concentration) of peak fluorescence at the well center. Curve *CF* is for carboxyfluorescein (in medium at pH 6.5) with a 3% transmittance neutral density filter in the excitation beam path. Curve *LRB* is for lissamine rhodamine B (in medium at pH 6.5) with the same neutral-density filter in the beam path. CF has a greater fluorescence yield on a molar basis than LRB when excited and analyzed by the appropriate interference filters in our microscope. The voltage output of the SIT camera at fixed gain is a linear function of dye concentration over a 60-fold range. At higher concentrations the response of the camera levels off gradually until it saturates. The right-hand ordinate gives the digitized light-intensity units derived from the voltages on the left-hand ordinate. The light intensities of experimental data are plotted as digital values.

In that the well forms a segment of a sphere, the fluorescence profile across it peaks at its center (Fig. 2).

During this calibration of the camera, and also during the experiments, the excitation beam from the HBO 50 lamp was adjusted by defocussing the lamp image at the object plane until the area of the microscope field in which fluorescence intensities were sampled was uniformly illuminated. This was achieved by exciting a uniformly thick region of dye solution (adjacent to the microrefractometer well) and defocussing the beam until the video signal sampled by the vertical cursor of the video analyzer gave a flat trace on an oscilloscope screen. When evenly illuminated, concentrations of CF in the test well as low as 10^{-8} M could be detected by the SIT camera.

The dynamic range of the SIT camera at fixed gain is reported to be between × 500 and 1,000 (34). We found the useful range of our camera to be slightly more than × 200 and the range over which the response was strictly proportional to dye concentration to be ~× 60 (Fig. 2).

The microrefractometer was a convenient test chamber as its maximum depth is similar to the thickness of the cell sheets into which dyes were injected. Also, the profile of light intensity across the well resembled to some extent the intensity profiles seen in the cell sheets, so that the camera was calibrated with images not unlike the experimental ones.

Because the diameter of the circle of light seen by the camera changes as the tracer spreads, it was also necessary to determine whether the SIT camera responded constantly to a circle of light of known intensity but variable diameter. A series of circles comparable with those seen in dye spreads was obtained on the TV monitor by using the image of the field diaphragm at × 6.3 (numerical aperture 0.20) objective magnification. For each field diaphragm diameter, the relationship between light intensity and camera response was measured by placing a series of neutral density filters (Kodak Wratten filters, No. 96, neutral density = 0.1–2) in the light path. Except for very large diameters (i.e., diameters that filled the video screen), the relationship remained constant.

Relationship between Dye Concentration and Fluorescence Emission: The practical range of cytoplasmic concentration of a fluorescence tracer used to determine its effective diffusion coefficient in a tissue is limited by several factors. The upper end of the range is set by the dye concentration above which concentration-dependent quenching (self-quenching or the inner-filter effect) occurs, and the relationship between dye concentration and fluorescence emission becomes nonlinear. Because tracer concentration is highest at the source in a typical dye spread, quenching would result in the SIT camera detecting reduced fluorescence in this region. When tested in the microrefractometer well, we found that no quenching of CF in medium at pH 6.5 occurred below 2×10^{-4} M. With a 3% transmission neutral density filter in the excitation path, the SIT camera was able to detect 10^{-6} M CF and saturated at 2×10^{-4} M (Fig. 2). The response range of the SIT camera was therefore fixed below quenching levels.

Photobleaching (fading) of dye during the sampling period was assessed by examination of the decay in fluorescence over 60 s of continuous excitation of known dye concentrations in the test well, in that measurements were usually of this duration. With this 3% neutral density filter in the excitation path, photobleaching lowered the initial fluorescence intensity of CF concentrations below 6×10^{-5} M by <10%. LRB was an even more stable dye when tested this way. Its fluorescence emission, over the concentration range 1×10^{-5} to 6×10^{-4}, remained within 2% of the initial value after 60 s of excitation with the reduced beam. The effective diffusion coefficients of CF and LRB were therefore determined within these concentration ranges, with this 3% neutral density filter in the light path.

Theory of Analysis of the Spreads of Fluorescent Tracer: The rate at which diffusion occurs is usually expressed in terms of a diffusion coefficient (10) that relates flux of material to its concentration gradient. The geometry of the epidermis and the method of injection of tracer allow its movement to be described in terms of the diffusion of material from a continuous line source in two dimensions, characterized by the equation:

$$C(r, t) = \frac{S}{4\pi Dh} \mathrm{Ei}\left(\frac{r^2}{4Dt}\right), \quad (1)$$

where $C(r,t)$ is the concentration of material (here a fluorescent tracer) at a distance r from the source at a time t from the start of injection, S is the delivery rate of the material, D is its diffusion coefficient, h is the thickness of the two-dimensional sheet in which the material is diffusing (here the height of the monolayer of cells), and π is a constant (5, 37). Initially, the concentration of tracer is zero. At $r = 0$ and $t = 0$ a constant tracer delivery (S) begins. The concentration at infinity approaches zero. Since S is in moles per second, h in centimeters, and D in centimeters^2 per second, the term $S/4\pi Dh$ has units of concentration, moles per cubic centimeter. If the dimensionless ratio $x = r^2/4Dt$ is small (i.e., $0 < x < \pi$, reference 1) the exponential integral (Ei) has the series expansion:

$$\mathrm{Ei}(x) = -\gamma - \ln(x) - \sum_{n=1}^{\infty} \frac{(-1)^n x^n}{n \cdot n!}, \quad (2)$$

where γ is Euler's constant (0.5772). For values of $x < 0.1$ ($0 < x < 0.1$), Eq. 1 becomes the following logarithmic function:

$$C(r, t) = \frac{S}{4\pi Dh} \ln\left(\frac{4Dt}{r^2}\right) - \frac{\gamma S}{4\pi Dh}, \quad (3)$$

which upon rearrangement gives:

$$C(r, t) = \frac{S}{4\pi Dh} \ln\left(\frac{4t}{r^2}\right) + \frac{S}{4\pi Dh} [\ln(D) - \gamma], \quad (4)$$

(an equation of the form $y = m \ln(x) + b$; i.e., a plot of y vs. $\ln(x)$ gives a straight line of slope m and y-intercept of b [at $\ln(x) = 0$]). A plot of concentration (expressed here as light intensity, since camera response is proportional to dye concentration over most of its useful range; see section on camera calibration) vs. $4t/r^2$ on semilog paper gives a straight line with

$$m = \frac{S}{4\pi Dh} \quad (5)$$

and

$$b = \frac{S}{4\pi Dh} [\ln(D) - \gamma]. \quad (6)$$

The y-intercept can be rewritten as

$$b = m [\ln(D) - \gamma], \quad (7)$$

which can then be rearranged to give an equation for calculating the diffusion coefficient of the material (D):

$$D = e^{[(b/m) + \gamma]}. \quad (8)$$

Similarly, D can be calculated using the x-intercept.[2] In this situation:

$$D = \frac{e^{\gamma}}{x\text{-intercept}}. \quad (9)$$

D calculated in either way is independent both of sheet thickness and of the rate at which the material is delivered. If we assume $4Dt/r^2$ to be >10 ($x = r^2/4Dt < 0.1$, as mentioned above), it follows that the curves generated by the exponential integral function and the logarithmic function superimpose at $\sim 4t/r^2 > 2 \times 10^7$, for values of $D < 5 \times 10^{-7}$ cm^2/s. Consequently, only points on the logarithmic curves (see Figs. 4*c*, 6*b*, 7*a*, and 8*a*) $>2 \times 10^7$ s/cm^2 were used to determine slope m.

The diffusion coefficient for tracer in the epidermis is a total or effective diffusion coefficient (D_e) and combines diffusion through cytoplasm and diffusion via membrane channels (48).

RESULTS

Diffusion of Fluorescent Molecules in the Epidermis

CARBOXYFLUORESCEIN: The movement of CF from cell to cell under normal conditions is quite rapid in both newly ecdysed and intermolt (5–7 d after ecdysis) epidermis. Within a few seconds of electrode penetration, this tracer spreads from the source (zero-order) cell to adjacent cells. With continuous injection, the tracer could be detected in fifth- or sixth-order cells by 1 min. Fig. 3, *a–f* shows the spread of CF over a period of just over 1 min in newly ecdysed epidermis. The spatial pattern of fluorescence due to tracer spread (shown as a function of time in the sequence of micrographs of Fig. 3) was digitized from the recorded images. The profile of fluorescence intensity across the center of a typical CF spread (a "topographic" plot [19] because it represents a topographic scan of light intensity) and the increase in this profile with time is shown in Fig. 4*a*. Tissue autofluorescence, with the CF excitation/emission filters in the light path, accounted for <5% of the range of digital light intensities measured. The same information is plotted to show the increase in light intensity at selected distances from the source with time in Fig. 4*B*. The linear portions of these curves have the same slope regardless of the distance from the source cell, a feature predicted by Eq. 3. The D_e of CF in the epidermis can be calculated from the slopes and y-intercepts of these lines by a modification of Eq. 3 (see legend to Fig. 4*b*). Because Fig. 4*b* shows that a given light intensity is repeated at distances farther from the source as the period of injection increases, it proved more expedient to calculate D_e from light intensity values plotted as in Eq. 4, namely as a function of both variables simultaneously. This analysis is seen in Fig. 4*c*. The entire two-dimensional matrix of fluorescence values sums onto one curve. In practice, only the values from one side of the profile of tracer fluorescence were used to calculate the effective diffusion coefficient. From the slope and the y-intercept of the straight line drawn through the linear portion of the curve in Fig. 4*c*, D_e for CF in this preparation was calculated using Eq. 8 as 3.5×10^{-7} cm^2/s.

It is possible, using this value of D_e to compare the full relationship, as predicted by Eq. 1, between light intensity and $4t/r^2$ with the actual data. The relationship predicted by Eq. 1 is shown as a dashed line in Fig. 4*c*. There is agreement between the light intensities for different values of $4t/r^2$ obtained in theory and in practice. At low values of $4t/r^2$, the theoretically predicted light intensities and those obtained experimentally climb slowly until the slope becomes linear. In the linear region, the exponential integral (Eq. 2) and the logarithmic approximation (Eq. 8) become indistinguishable.

There also appears to be a stage-specific localization of CF in certain organelles. In newly ecdysed epidermis, CF binds to irregularly shaped structures, giving a mottled appearance to the fluorescence image (Fig. 3). The spread of CF in intermolt cells (Fig. 5*b*) is qualitatively different from that in newly ecdysed cells inasmuch as tracer is localized more in the nuclear region. CF did not enter damaged cells and cytoplasmic vacuoles. These were rare and any region in the tissue containing them was avoided in the quantitative analysis.

LISSAMINE RHODAMINE B: Compared with CF, both the qualitative appearance and the rate of LRB movement in the epidermis differ (Fig. 5). The cell-to-cell spread of LRB is more homogeneous, as it binds less than CF to cytoplasmic organelles. Consequently, the intensity of LRB fluorescence within each cell is fairly uniform, and as the local tissue concentration of the tracer builds up during injection, small downward "steps" in fluorescence, corresponding to successive orders of cells, become visible in the video image (Fig. 5*c*). These steps were not seen in the CF spreads, except when the rate of tracer movement in the epidermis was reduced experimentally (see below).

That the rate of movement of LRB (1.8 × 1.4 × 1.1 nm, channel-limiting dimension underlined[3]) is much slower than that of CF (1.2 × 1.2 × 0.8 nm). This is qualitatively evident from Fig. 5, *b* and *c*, which shows that the extent of the LRB spread is less than that of CF after the same period of tracer injection. Quantitatively, the topographic plots for LRB (Fig. 6*a*) are steeper than those for CF (Fig. 4*a*). For example, whereas CF fluorescence could be detected 30 μm from the source cell after 11 s of injection (Fig. 4*a*), LRB fluorescence could not be detected beyond 20 μm at this time (Fig. 6*a*).

[2] We thank J. D. Sheridan and M. Atkinson of the University of Minnesota for pointing this out to us.

[3] Molecular dimensions were measured from CPK space-filling models with the channel-limiting dimensions being defined as the second largest of the measurements.

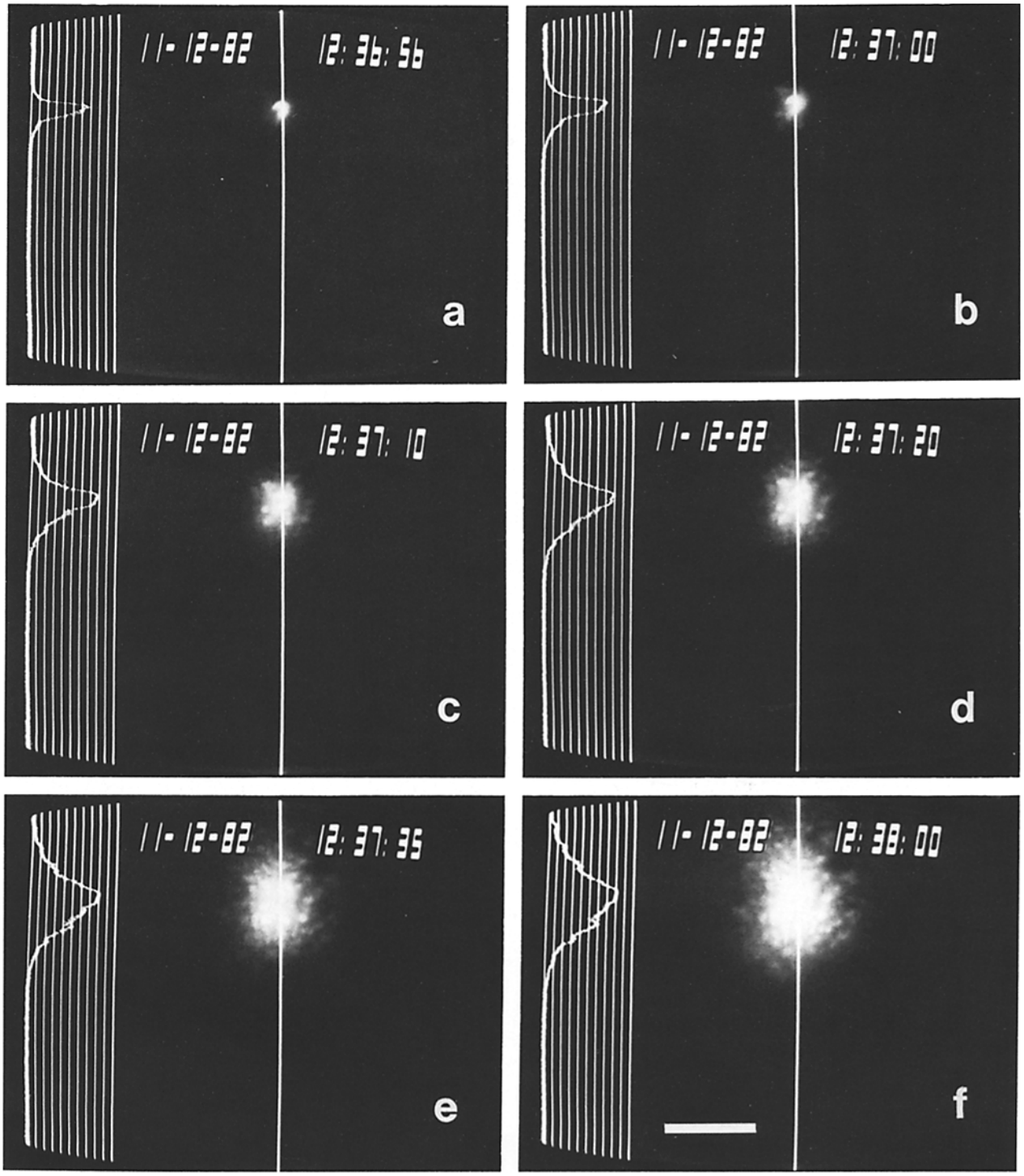

FIGURE 3 Video images of CF spreading in the epidermis. This sequence of photographs records the spread of CF at different times after the start of injection in newly ecdysed epidermis. Injection began at 12:36:53. At the left of each photograph the slowscan output gives the light intensity along the vertical cursor positioned across the center of the dye spread. The mottled appearance to the spread of CF is characteristic of this stage in development. *a* is the image after CF had been injected into the source cell for 3 s, while in *f* the extent of spread after 67 s is shown. Bar, 50 μm. × 300.

Tissue autofluorescence, using the LRB excitation/emission filters, was <10% of the range of digital light intensities measured.

The $4t/r^2$ curve for LRB is shifted to the right (Fig. 6*b*), compared with that of CF (Fig. 5*c*). As a rough indicator, the further to the right the curve, given comparable slopes, the lower the effective diffusion coefficient calculated from Eq. 8. The LRB curve in Fig. 6*b* corresponds to a D_e of 1.0×10^{-7} cm^2/s.

The calculated D_e's for CF and LRB in newly ecdysed and intermolt tissues are summarized in Table I. The diffusion coefficient of CF in intermolt tissue is higher than that in newly ecdysed tissue, and at both developmental stages greater than LRB. Occasionally, the movement of both tracers was

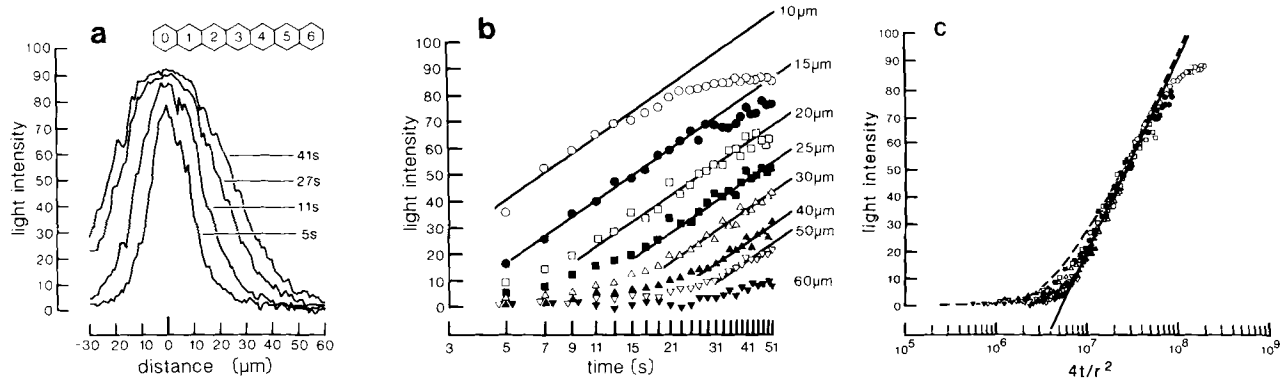

FIGURE 4 Analysis of carboxyfluorescein spreads. (*a*) Topographic plot. The spatial distribution of CF fluorescence, plotted as digital light intensities, was sampled along a line through the center of the dye spread. The data are plotted at 1-μm intervals for 5, 11, 27, and 41 s of injection into newly ecdysed tissue. A row of idealized cells drawn to scale above these curves shows that CF had entered the sixth order cells by 41 s. (*b*) The digital light intensities (Li) plotted against log(time) show the following linear relationship at selected distances (r) from the source: $Li = (S/4\pi D_e h) \ln(t) + (S/4\pi D_e h)(\ln[4 D_e/r^2] - \gamma)$. The mean D_e calculated from the lines drawn through the sets of points is 3.4 (± 0.2) × 10^{-7} cm^2/s. (○, 10 μm; ●, 15 μm; □, 20 μm; ■, 25 μm; △, 30 μm; ▲, 40 μm; ▽, 50 μm; ▼, 60 μm). Near the source cell (such as at 10 and 15 μm), where high light intensities are seen, the points fall away from the predicted relationship because of the response characteristics of the camera (see Fig. 2). Further from the source (as seen at 50 μm) light intensities increase slowly with time (as predicted by Eq. 1) until the linear relationship given above holds. (*c*) $4t/r^2$ plot. When the light intensities are plotted against $4t/r^2$ all the data points fall on a single curve. The data plotted here and the symbols used are the same as in *b*. From the maximum slope (30.8, using natural logarithms) and y-intercept (−476) for the solid line drawn by eye through these points, a D_e of 3.5 × 10^{-7} cm^2/s was calculated (see Eq. 7). The dashed line represents the exponential integral evaluated for this D_e. A simplified form of Eq. 2 for programmable calculators found in reference 26 (pp. 61–63) was used.

analyzed from spreads in the same piece of epidermis (Fig. 5). In one intermolt preparation, a series of four CF spreads was bracketed by seven LRB spreads over a period of 45 min. The D_e's for the CF spreads ranged from 2.6 to 4.0 × 10^{-7} cm^2/s whereas those of the five LRB spreads done before the CF spreads ranged from 0.7 to 0.9 × 10^{-7} cm^2/s and the two after were 0.9 and 1.0 × 10^{-7} cm^2/s. The mean ratio of D_e for these two tracers was about 3. The ratios derived from many preparations at both stages of development are given in Table I.

Influence of Tracer Delivery Rate and Iontophoretic Current on D_e

The rate of delivery of fluorescent tracer into the epidermis may be varied by alteration of the iontophoretic current. In theory the delivery rate does not influence D_e (Eq. 3), but the train of current pulses used to drive tracer from the electrode into the source cell may also affect its movement in the tissue. Although tracer movement is not dependent on the pulses of electrotonic current that spread radially away from the source cell into the tissue during injection—tracer continues to move when the current is turned off—the spread of current during injection of tracer may raise its effective diffusion coefficient.

The influence of different current strengths on the delivery rate of CF (a negatively charged tracer) into the epidermis is shown in Fig. 7, *a* and *b*. Increasing the iontophoretic current raises the rate of injection and consequently the light intensity at any selected combination of time and distance from the source. The D_e calculated from the lower three curves in Fig. 7*a*, 2.2–2.5 × 10^{-7} cm^2/s, suggests that it is not influenced by the tracer delivery rate. It was noted, however, that the iontophoretic current associated with the fastest delivery rate appeared to raise D_e, to 4.3 × 10^{-7} cm^2/s (top curve in Fig. 7*a*). Fig. 7*a* is in agreement with theory that predicts that for constant D but increasing dye delivery, the slope of the $4t/r^2$ curve changes but the x-intercept does not.

To study the effects of iontophoresis in more detail, current strengths ranging from 0.1 to 10 nA were tested, and the results are summarized in Fig. 7*b*. The length (0.2 s) and the frequency (one per second) of the current pulses were kept constant. Increasing the current strength 100 times raised D_e only 1.6 times. Indeed, the slight slope to the regression line through the data in Fig. 7*b* may not be due entirely to iontophoretic effects, but to camera saturation beyond the source cell when strong currents are used (see Discussion). The extrapolation to zero current in Fig. 7*b* gives the D_e for CF as 2.3 × 10^{-7} cm^2/s, which is within the range of error for D_e of this tracer determined when the standard current strength of 6 nA was used.

Influence of Chlorpromazine on the Rate of Diffusion of CF

The calmodulin antagonist chlorpromazine (CPZ) raises junctional resistance in the epidermis. After 20 min of exposure to 0.25 mM CPZ, the ionic resistance of the intercellular pathway increases several fold and ionic coupling between the cells is lost by ~40 min (20). Furthermore, the normal cell-to-cell movement of CF is abolished by this treatment; dye fails to pass out of the cell into which it is injected when the cells are ionically uncoupled (see Fig. 2 in reference 20; see also Fig. 9). To what extent can this method follow the changing D_e of CF as the epidermis uncouples during CPZ treatment?

Qualitative changes in the cell-to-cell spread of CF in CPZ-treated epidermis, compared with its spread in control epidermis, were first detected after 10–15 min of exposure. The spread of CF by this time began to resemble that of LRB in normally coupled tissue (Fig. 5*c*), i.e., the tracer increases in

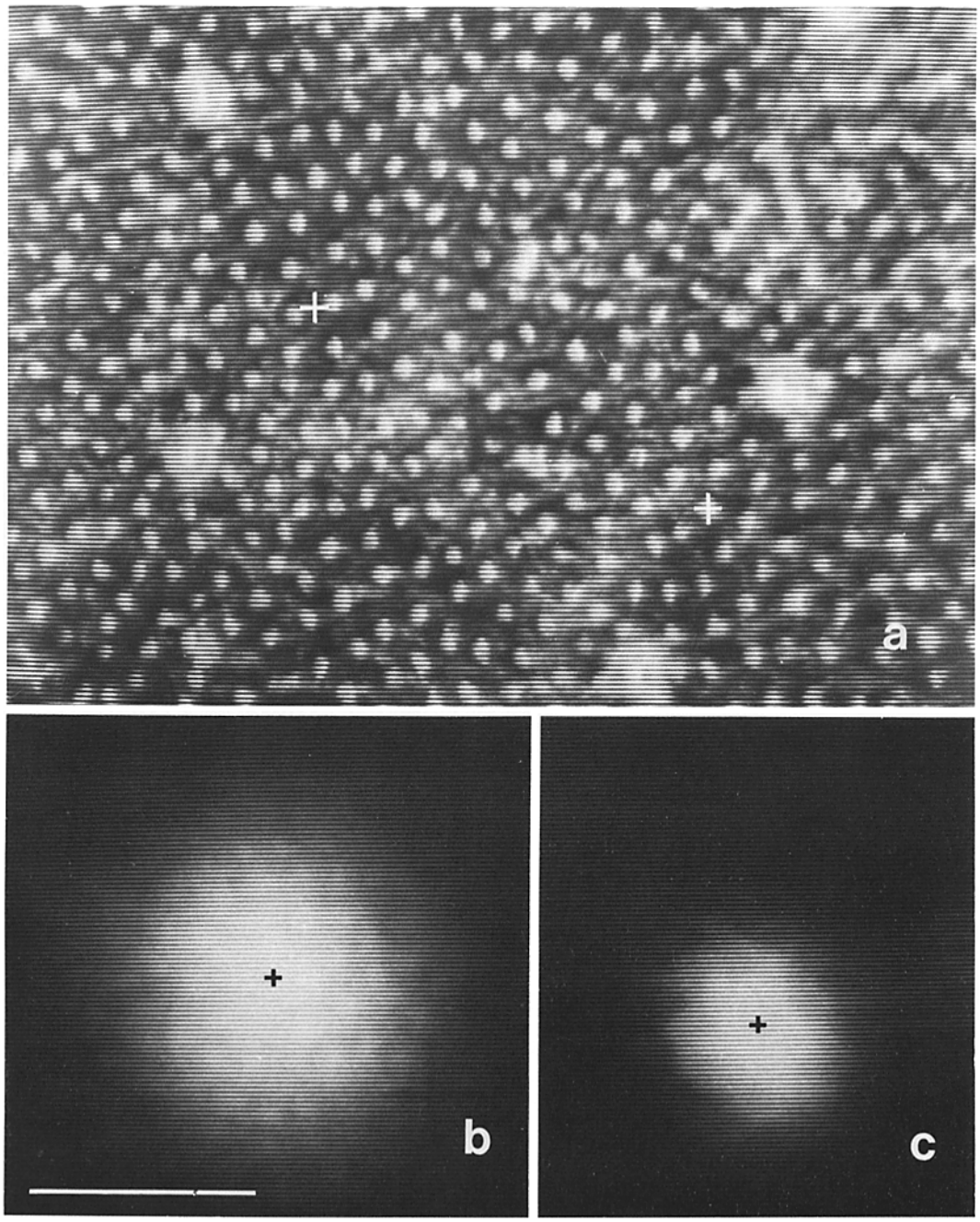

FIGURE 5 Comparison of the rate and appearance of spread of CF and LRB in a single intermolt preparation. Sites of tracer injection are marked by a cross (+). Both fluorescence micrographs (*b*) and (*c*) were taken from the video-taped images after 30 s of tracer injection. (*a*) Phase-contrast image of the epidermal cells in which the lighter nuclei are seen to stand out against the darker cytoplasm. The white crosses (+) mark the sites of injection of CF (upper left, shown in *b*) and LRB (lower right, shown in *c*). The four blurred spots in the phase image are sites of sensory structures. (*b*) Spread of CF. The dye had spread five to six orders of cells in 30 s. While spreading rapidly from cell to cell, CF did not appear to be impeded by the cell borders but did localize in the nuclear regions of cells. (*c*) Spread of LRB. LRB had spread less than CF in 30 s and imaged only the first three orders of cells. With this dye it was possible to distinguish the different orders of cells around the source cell and their boundaries. Here, the source cell is surrounded by five first-order cells arranged in a five-pointed star. The fluorescence image shows a uniform fluorescence within these five first-order cells, and a lower fluorescence in the second-order cells. The effective diffusion coefficients calculated from the video-taped sequences of these two spreads were 3.9×10^{-7} cm^2/s for CF and 1.9×10^{-7} cm^2/s for LRB. Bar, 50 μm. × 640.

concentration uniformly in each order of cells before substantial movement into the next order is seen. By 20 min of CPZ treatment, the passage of CF out of the source cell had become very slow, and almost a minute lapsed before CF built up in concentration in the first order cells. The decrease in the rate of CF movement in the epidermis during exposure to CPZ is shown quantitatively in Fig. 8. During drug treatment, the $4t/r^2$ curves shift to the right and their slopes become progressively greater (Fig. 8*a*). For decreasing D, but constant dye delivery, Eq. 4 predicts that the slopes of the $4t/r^2$ curves

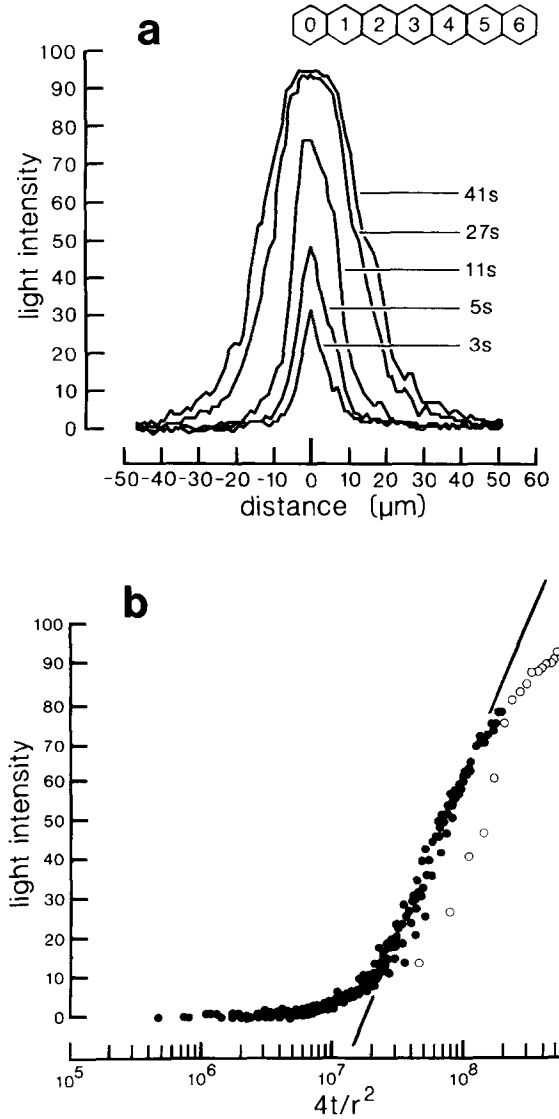

FIGURE 6 Analysis of LRB spreads. (a) Topographic plot. The spatial distribution of LRB fluorescence is plotted as in Fig. 4a, for tissue at the same stage in development. The light-intensity profiles are more acute than those of CF when analyzed after the same periods of injection. (b) $4t/r^2$ plot. Light intensities are plotted against $4t/r^2$ for the distances listed in Fig. 4b, except that the 60-μm values have been omitted. Compared with the CF curve of Fig. 5c, the curve here is displaced to the right and its maximum slope is slightly steeper. D_e calculated from this curve is 1.0×10^{-7} cm²/s. The light intensities measured at 5 μm from the source do not fall on the curve. In general, light intensities at distances <10 μm from the source did not fall on the $4t/r^2$ curves and were not included in the calculation of D_e. The reasons for this are given in Discussion.

TABLE I

D_e's of Two Fluorescent Molecules in the Epidermis

Molecule	D_e	
	Newly ecdysed epidermis	Intermolt epidermis
	$\times 10^7$ cm²/s	
CF	2.7 ± 0.8 (83, 16)*	3.7 ± 1.0 (100, 23)
LRB	1.2 ± 0.4 (29, 7)	1.2 ± 0.4 (23, 5)
D_eCF/D_eLRB	2.3	3.1

* Mean ± SD (number of spreads analyzed, number of preparations used).

increase and the curves tend to shift to the right along the *x*-axis. D_e dropped from 5.0×10^{-7} cm²/s to ~1×10^{-7} cm²/s over a period of 30 min (Fig. 8*b*). Dye coupling was lost after 30 min (Fig. 9), but by this time drug treatment had made it difficult to hold the membrane potential of source cells for longer than 30 s and so the test periods were shorter.

Cell uncoupling with CPZ also allowed us to determine the lowest D_e that can be reliably measured by this method. The successful passage of dye from a source cell to its neighbors can be scored with confidence only if the distance is known over which stray fluorescence from the out-of-focus regions around the source cell superimpose on the focussed image. Since the depth of field of the × 40 objective (1–2 μm) is less than cell height, out-of-focus fluorescence inevitably spreads beyond the source cell. To establish how far, CF was injected continuously into several CPZ uncoupled cells for 50 s and the fluorescence profile across each cell recorded during injection. Fig. 9 plots the fluorescence intensity across an uncoupled cell at 7 and 27 s of injection. Although fluorescence drops abruptly at the cell margin (see micrograph above Fig. 9) some out-of-focus light spreads into the first-order cells, but this drops to <10% of the value at the edge of the cell over a distance of 8–9 μm, i.e., within the first-order cells. This shoulder to the fluorescence profile was seen to climb during the first 20 s of injection, and then remain constant. If the dye had been actually diffusing among the cells the shoulder would have increased in height throughout the injection period (e.g., Figs. 4 and 6). The D_e of a tracer was only calculated when fluorescence intensity increased in at least the second-order cells during the sampling period (maximum length 2 min). The lowest D_e measured for CF, by this criterion, was about 7×10^{-8} cm²/s.

DISCUSSION

The rates of diffusion of CF and LRB via intercellular membrane channels are quite rapid. Diffusion coefficients of these tracers in the epidermis are only an order of magnitude lower than those for molecules of similar molecular weight in water (compare reference 45). For example, *D* for sucrose (342 mol wt) in water at 20°C is 4.6×10^{-6} cm²/s (43). Our findings are consistent with previous measurements of D_e presented in Table II. The values in this table reflect the trend towards lower diffusion coefficients with increasing molecular weight. It is interesting to note that this decrease in D_e is greater than that predicted from molecular weight alone and probably reflects restriction by channels with a finite diameter. Factors other than molecular weight, such as molecular charge (4, 14), may also affect the rates of movement of molecules from cell to cell.

We have investigated several possible sources of error in our measurement of D_e. It is possible that some error is involved in determining the distance from the source and times from the start of injection. Since *r* and *t* are determined precisely by counting horizontal (TV lines) and vertical synchronization (TV fields), respectively, any inaccuracies lie in determining *r*(0), the source cell, and *t*(0), the start of injection. If the site of the electrode tip is misjudged or the electrode drifts within the source cell during injection, distances from the source cell will be offset. A vertical displacement of up to 5 μm either side of the source results in an error of up to 0.5×10^{-7} cm²/s. (This was determined by purposely shifting *r*(0) and then determining D_e.) In this case, however, the $4t/r^2$

TABLE II

D_e's for Molecular Movement among Cells in Several Tissues

Molecules	Molecular weight	D_e	Tissue (reference)
	D	$\times 10^{-7}$ cm^2/s	
K^+	39	79	Sheep ventricular fibers (48)
Tetraethylammonium	130	20	Sheep and calf ventricular fibers (49)
2-deoxyglucose	190	17*	Rat myometrial smooth muscle (9)
		1.7‡	
Cyclic AMP	329	8.4	Calf ventricular muscle (42)
Fluorescein	333	40	Canine Purkinje fibers (12)
		10	Earthworm median giant axon (4)
CF	376	2.7–3.7	This paper
Diiodofluorescein	490	0.5	Earthworm median giant axon (4)
Dibutyryl cAMP	491	5.9	Calf ventricular muscle (42)
LRB	559	1.2	This paper
Tetrabromofluorescein	652	0.1	Earthworm median giant axon (4)
Procion yellow	697	0.3	Sheep and calf Purkinje fibers (16)

* Parturient rats.

‡ Control rats.

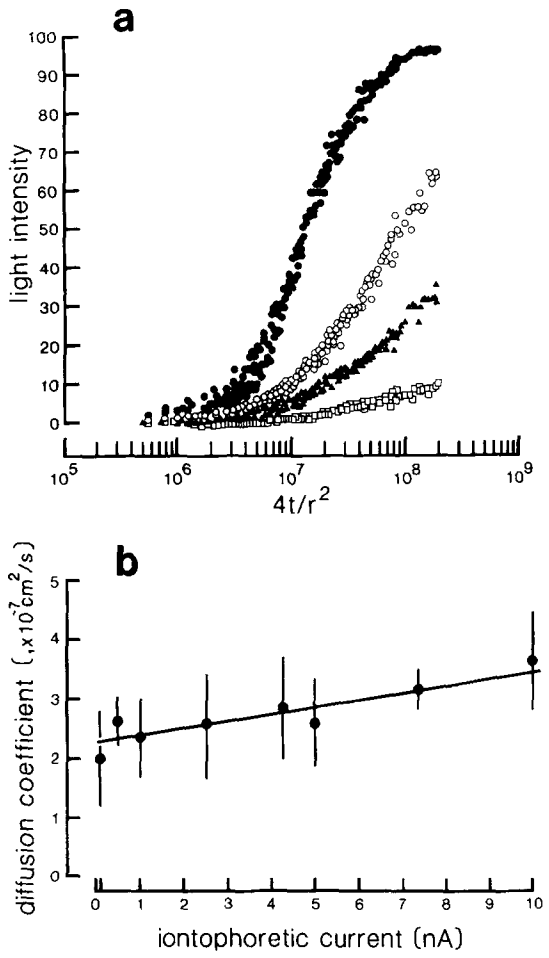

FIGURE 7 Influence of the rate of delivery (*a*) and strength of the iontophoretic current (*b*) on the D_e of CF in newly ecdysed epidermis. (*a*) $4t/r^2$ plots of CF spreads in the epidermis of one animal at four different rates of delivery. The initial rise in all four curves occurs at about the same point along the *x* axis (compare Fig. 9*a*). The rate of delivery was increased by raising the iontophoretic current. The current strengths and calculated D_e's for the four curves are (□) 0.5 nA, 2.5×10^{-7} cm^2/s; (▲) 1 nA, 2.2×10^{-7} cm^2/s; (○) 5 nA, 2.4×10^{-7} cm^2/s; and (●) 10 nA, 4.3×10^{-7} cm^2/s. (*b*) The D_e for CF climbs slightly as the iontophoretic current is raised. The line drawn through the points (means ± SD, total $n = 63$) has a slope of 1.2×10^{-8} cm^2/s-nA and a *y*-intercept of 2.3×10^{-7} cm^2/s.

plots differ from those presented in this paper, i.e., the points no longer fall on one curve. A horizontal error of up to 2 μm on either side of the source (created by moving the cursor of the video analyzer laterally) had little effect on D_e. An error in determining the start of injection equal to the sampling interval also had minimal effect on D_e (0.2×10^{-7} cm^2/s for an error of ±2 s). Much of the error associated with determining light intensities occurred when fluorescence intensities very close to the source were measured. As a rule, values for D_e were determined from light intensities sampled at 1-μm intervals between distances 10–70 μm from the center of the source cell. Light intensities <10 μm from this cell were not included in the analysis because (*a*) they may have resulted from sampling points lying inside the source cell, and thus the light intensities reflect cytoplasmic D rather then D_e; (*b*) the diffusion of tracer at distances from the electrode tip (a point-source) less than the sheet thickness was three dimensional and not two dimensional as required by the theory; (*c*) values near the source tended to lie in the nonlinear portion of the camera response; and (*d*) excessive rates of tracer delivery into the tissue, leading to camera saturation in and around the source cell in normally coupled tissues, may raise artificially the calculated D_e (Fig. 7*a*, top curve). Points such as those illustrated in Fig. 6*b* (open circles) are eliminated by not including light intensities sampled closer than 10 μm to the source. We found that provided the camera saturation did not extend beyond the source cell, the D_e's determined for a given tracer at a selected stage in development were consistent.

In that dye was delivered by iontophoresis, could electrical current influence the rate of dye movement among the cells? Fig. 7*b* shows that there is a slight effect on D_e although it may be argued that there is no influence until the current exceeds 7 nA. That iontophoretic delivery has little or no effect on molecular diffusion has also been observed in brain tissue where predictions from "diffusion alone" matched observations (30). In our experiments, an iontophoretic current of 6 nA was chosen because it delivered dye into the tissue at a rate sufficient to obtain a measurable dye spread within 2 min of injection, yet cause minimal camera saturation in the region of the source cell. Although we have used pulses of iontophoretic current and not "constant" delivery as assumed by the theory, we found it unnecessary to modify the model to include periodic sources. Occasionally, small pulsatile increases in fluorescence were observed beyond the source cell.

These contributed to the scatter or the $4t/r^2$ plots, but did not alter their general appearance.

An assumption made in this paper is that membrane junctions are the major barrier to molecular movement among epidermal cells. It does not necessarily follow, however, that changes in D_e of a tracer during development are due entirely

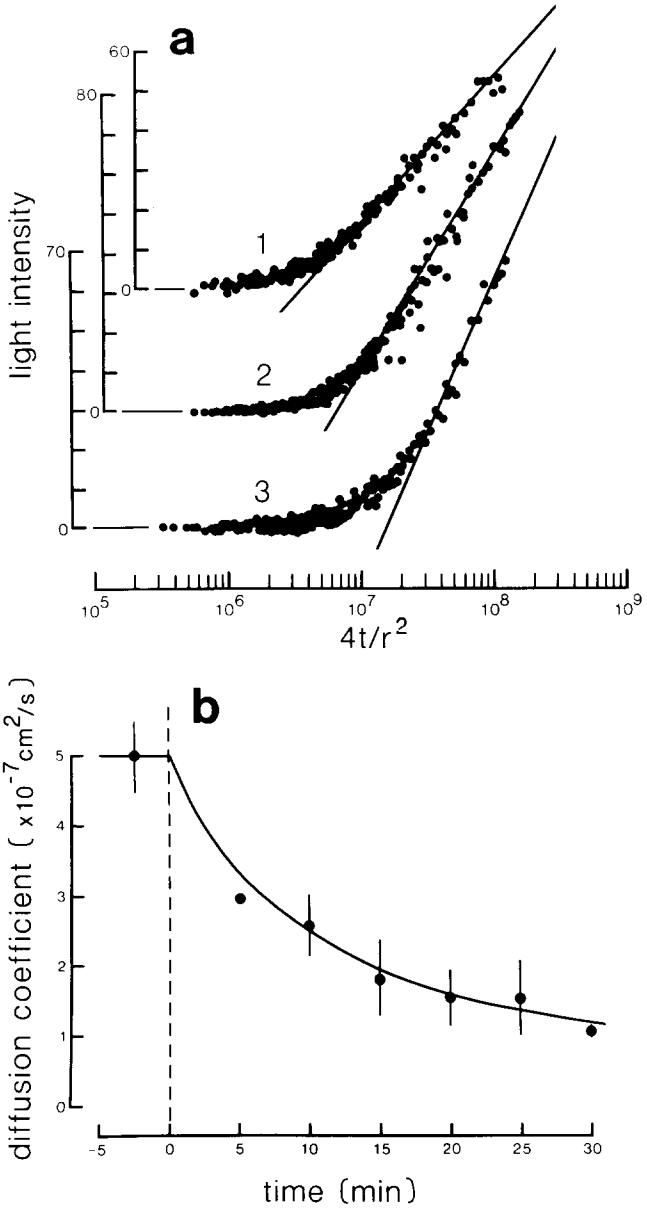

FIGURE 8 Influence on D_e of changes in intercellular resistance in intermolt epidermis. (*a*) The $4t/r^2$ plot for the epidermal preparation in control medium (curve *1*) has a shallow slope and a D_e of 4.8 × 10^{-7} cm^2/s. As the cells of this preparation uncoupled on exposure to 0.25 mM CPZ, the $4t/r^2$ curves became steeper and the position at which the curves rose shifted to the right. After 10 min of exposure (curve *2*) D_e had dropped to 2.7 × 10^{-7} cm^2/s and by 20 min (curve *3*) to 1.2 × 10^{-7} cm^2/s. (*b*) Time course of the change in D_e for CF after exposure to CPZ at time 0. D_e dropped rapidly from a control value of 5.0 × 10^{-7} cm^2/s down to 1.0 × 10^{-7} cm^2/s during 30 min of exposure to the drug. Intercellular resistance rises over this 30-min period (not shown). The data shown were obtained from four preparations taken from three animals and are the means (±SD) of 12 spreads analyzed before the drug was applied and 30 spreads analyzed in its presence.

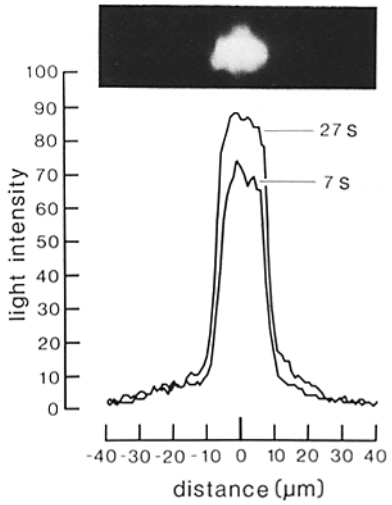

FIGURE 9 Out-of-focus and scattered-light effects on the image of a dye-uncoupled cell. CF was injected into a cell in intermolt epidermis uncoupled by exposure to 0.25 mM CPZ for >30 min. Fluorescence intensities measured across this cell are shown at 7 and 27 s from the start of injection. The cell, 13–15 μm wide along the line sampled, is shown at the same scale in the micrograph above the figure. The low levels of light intensity at the cell's margins are not due to dye diffusion but to either light scattered by the cuticle (through which the cell is viewed) or to dye-filled regions of the cell that are above and below the focal plane of the objective (see text for details).

to changes in junctional permeability, since tracer localization within cellular components may vary. For example, the lower D_e for CF seen in newly ecdysed epidermis when compared with intermolt epidermis (Table I) may be a consequence of greater dye localization at this time. Localization of a dye (whether by binding or sequestration) will lower its effective diffusion rate because D_e is a function of both cytoplasmic diffusion (which is reduced by dye localization) and cell-to-cell diffusion, where $1/D_e = 1/D_{cytoplasm} + 1/D_{channel}$ ($D_{channel}$ being a complex term that considers tissue geometry, channel number, and permeability). If $D_{cytoplasm}$ and $D_{channel}$ are of equal magnitude, then an increase, e.g., a doubling, of either one will raise D_e to the same extent. If, on the other hand, $D_{channel}$ is considerably less than $D_{cytoplasm}$, doubling $D_{channel}$ will have a much greater effect on D_e. The cytoplasmic diffusion coefficient of a tracer must be known before developmental changes in D_e can be attributed to changes in junctional permeability. Nevertheless, the junctions do appear to be the major determinant of D_e, because (*a*) there is a correlation between decreased junctional conductance to ions and decreased permeability to tracers at a given stage in development when the cells are uncoupled by CPZ (see Results) and (*b*) the cytoplasmic diffusion coefficient for CF within cells of the epidermis is as high as 2 × 10^{-6} cm^2/s. (A preliminary value obtained by fluorescence photobleaching recovery of the cytoplasm of intermolt epidermal cells preloaded with CF diacetate, in collaboration with Dr. Nils Petersen, Department of Chemistry, University of Western Ontario; CF diacetate is a nonfluorescent membrane permeable dye that is hydrolyzed to fluorescent impermeable CF [31].)

The ratio of the predicted cytoplasmic D's for CF and LRB, based on molecular size, is almost unity (1.1). The cytoplasmic D's for CF and LRB predicted by the Stokes–Einstein equa-

tion ($D = kT/6\pi nr$; reference 40) are 1.2 and 1.1 × 10^{-6} cm^2/s, respectively ($k = 1.38 \times 10^{-23}$ J/deg K; $T = 300$°K; r = half the limiting dimension of CF [0.6 nm] or LRB [0.7 nm]; and the viscosity $n = 3 \times 10^{-3}$ N-s/m^2, three times that of water; reference 41) Yet the ratio of D_e for these two tracers in newly ecdysed and intermolt tissue is between 2 and 3 (Table I). The lower ratio for newly ecdysed cells is most likely due to the stronger localization of CF in cytoplasm at this stage in development. LRB does not localize in the cells at either stage. The channels appear to impede differentially the movement of the slightly larger LRB molecule. (It has been reported that LRB is a neutral molecule and that CF is negatively charged [25]. We do not eliminate the possibility that this discrimination is related to molecular charge.) In models of cell patterning that involve morphogen diffusion (19, 26), changes in the D_e ratio can influence the spacing of the pattern elements (29). In hydra, pairs of diffusible morphogens have been found. It is suggested that lower molecular weight "inhibitors" pass more easily through the cell-to-cell channels than the larger "activators" (15). The channels may amplify the difference in the rates of movement, and increase the D ratio to the levels required by the models (29). Whether the D_e ratio for small cytoplasmic molecules is regulated by developing cells remains to be shown.

Nevertheless, the rapid rates of molecular diffusion in tissues reported here are of considerable relevance to development. Crick (11) predicted that a morphogen would require a D_e of ~2 × 10^{-7} cm^2/s to allow a concentration gradient based on simple diffusion to be set up in the few hours available for pattern formation (52). Lack of direct measurements of D_e in developing tissues has encouraged speculation that this rapid rate of diffusion could only be achieved by inorganic ions (in spite of evidence from cardiac muscle), and that they may be the morphogens (46). Our results show that it may be premature to consider inorganic ions the only molecules capable of rapid cell-to-cell movement in developing tissues.

We are very grateful to Dr. Alan C. Groom and Dr. Christopher G. Ellis of the Department of Biophysics (University of Western Ontario) for generous use of their video analysis equipment in the early stages of this work, to Mr. Livio Rigutto for construction of our field counter, and to Dr. S. Inoué and the instructors of the quantitative light microscopy course given at Woods Hole for their helpful advice and suggestions. We also thank Michael Blennerhassett, Yves Ouellette, John Krayacich, and Marianne Talman for their critical comments and assistance, and to Rosemary Melchin for the typing of the manuscript.

This research was supported by operating and equipment grants from the Natural Sciences and Engineering Research Council of Canada and by an Academic Development Grant from the University of Western Ontario.

Received for publication 27 September 1983, and in revised form 30 July 1984

REFERENCES

1. Abramowitz, M., and I. A. Stegun. 1970. Handbook of Mathematical Functions. U. S. Government Printing Office, Washington, D. C. 229.
2. Bennett, M. V. L., D. C. Spray, and A. L. Harris. 1981. Gap junctions and development. *Trends Neurosci.* 3:159–163.
3. Blennerhassett, M. G., and S. Caveney. 1984. Separation of developmental compartments by a cell type with reduced junctional permeability. *Nature (Lond.).* 309:361–364.
4. Brink, P. R., and M. M. Dewey. 1978. Nexal permeability to anions. *J. Gen. Physiol.* 72:67–86.
5. Carslaw, H. S., and J. C. Jaeger. 1959. Conduction of Heat in Solids. Oxford University Press, Oxford. 261.
6. Caveney, S. 1978. Intercellular communication in insect development is hormonally controlled. *Science (Wash. DC).* 199:192–195.
7. Caveney, S., and M. G. Blennerhassett. 1980. Elevation of ionic conductance between insect epidermal cells by β-ecdysone in vitro. *J. Insect Physiol.* 26:13–25.
8. Caveney, S., and C. Podgorski. 1975. Intercellular communication in a positional field: Ultrastructural correlates and tracer analysis of communication between insect epidermal cells. *Tissue Cell.* 7:559–574.
9. Cole, W. C., R. E. Garfield, and J. S. Kirkaldy. 1983. Increased gap junction area improved cell-to-cell diffusion of ^{3}H-2-deoxyglucose between uterine smooth muscle cells. *Biophys. J.* 41:84a. (Abstr.)
10. Crank, J. 1975. The Mathematics of Diffusion. Clarendon Press, Oxford.
11. Crick, F. H. C. 1970. Diffusion in embryogenesis. *Nature (Lond.).* 225:420–422.
12. DeMello, W. C. 1979. Effect of 2-4-dinitrophenol on intercellular communication in mammalian cardiac fibres. *Pflugers Arch. Eur. J. Physiol.* 380:267–276.
13. Ellis, C. G., R. G. A. Safranyos, and A. C. Groom. 1983. Television-Computer method for in vivo measurement of capillary diameter based on the passage of red cells. *Microvasc. Res.* 26:131–150.
14. Flagg-Newton, J., I. Simpson, and W. R. Loewenstein. 1979. Permeability of the cell-to-cell membrane channels in mammalian cell junction. *Science (Wash. DC).* 205:404–407.
15. Grimmelikhuijzen, C. J. P., and H. C. Schaller. 1979. Hydra as a model of organism for the study of morphogenesis. *Trends Biochem. Sci.* 4:265–267.
16. Imanaga, I. 1974. Cell-to-cell diffusion of procion yellow in sheep and calf purkinje fibres. *J. Membr. Biol.* 16:381–388.
17. Inoué, S. 1981. Video image processing greatly enhances contrast, quality and speed in polarization-based microscopy. *J. Cell Biol.* 89:346–356.
18. Kohen, E., and C. Kohen. 1978. The intercellular transfer of molecules in tissue culture cells: a kinetic study by multichannel microfluorimetry. *In* Differentiation and Development (Miami Winter Symposia, Vol. 15). F. Ahmad, J. Schultz, T. R. Russell, and R. Weiner, editors. Academic Press, Inc., New York. 411–439.
19. Lacalli, T. C., and L. G. Harrison. 1979. Turing's conditions and the analysis of morphogenetic models. *J. Theor. Biol.* 76:419–436.
20. Lees-Miller, J. P., and S. Caveney. 1982. Drugs that block calmodulin activity inhibit cell-to-cell coupling in the epidermis of Tenebrio molitor. *J. Membr. Biol.* 69:233–245.
21. Liu, T. F., E. Y. Kam, and J. D. Sheridan. 1982. Dye transfer through permeable junctions between cultured mammalian cells: quantitative video analysis. *J. Cell Biol.* 95 (2, Pt. 2):106a. (Abstr.)
22. Lo, C. W. 1980. Gap junctions and development. *In* Development in Mammals. Vol. 4. M. H. Johnson, editor. Elsevier/North Holland Biomedical Press, Amsterdam. 39–80.
23. Lo, C. W., and N. G. Gilula. 1979. Gap junctional communication in the post-implantation mouse embryo. *Cell.* 18:399–409.
24. Loewenstein, W. R. 1979. Junctional intercellular communication and the control of growth. *Biochim. Biophys. Acta.* 560:1–65.
25. Loewenstein, W. R. 1979. Junctional intercellular communication: the cell-to-cell membrane channel. *Physiol. Rev.* 61:829–913.
26. Meck, H. R. 1981. Scientific Analysis for Programmable Calculators. Prentice-Hall, Englewood Cliffs, N. J. 61–63.
27. Meinhardt, H., and A. Gierer. 1974. Applications of a theory of biological pattern formation based on lateral inhibition. *J. Cell Sci.* 15:321–346.
28. Michalke, W. 1977. A gradient of diffusible substance on a monolayer of cultured cells. *J. Membr. Biol.* 33:1–20.
29. Murray, J. D. 1982. Parameter space for Turing instability in reaction diffusion mechanisms: a comparison of models. *J. Theor. Biol.* 98:143–163.
30. Nicholson, C., and J. M. Phillips. 1981. Ion diffusion modified by tortuosity and volume fraction in the extracellular microenvironment of the rat cerebellum. *J. Physiol. (Lond.).* 321:225–257.
31. Petersen, N. O., and W. B. McConnaughey. 1981. Effects of multiple membranes on measurements of cell surface dynamics by fluorescence photobleaching. *J. Supramol. Struct. Cell. Biochem.* 17:213–221.
32. Pollack, G. H. 1976. Intercellular coupling in the atrioventricular node and other tissues of the rabbit heart. *J. Physiol. (Lond.).* 255:275–298.
33. RCA Service Manual. 1979. CCV-127A, TC1030/H, TC1040/H SIT and ISIT cameras. RCA Electro-Optics & Devices, Lancaster, PA. 5–12, 5–13, 5–15.
34. Reynolds, G. T., and D. L. Taylor. 1980. Image intensification applied to light microscopy. *Bioscience.* 30:586–592.
35. Rose, B., and W. R. Loewenstein. 1976. Permeability of a cell junction and the local cytoplasmic free ionized calcium concentration: a study with aequorin. *J. Membr. Biol.* 28:87–119.
36. Rose, B., I. Simpson, and W. R. Loewenstein. 1977. Calcium ion produced graded changes in permeability of membrane channels in cell junction. *Nature (Lond.).* 267:625–627.
37. Segel, L. 1980. Mathematical Models in Molecular and Cellular Biology. Cambridge University Press, Cambridge. 434.
38. Spray, D. C., A. L. Harris, and M. V. L. Bennett. 1979. Voltage dependence of junctional conductance in early amphibian embryos. *Science (Wash. DC).* 204:432–434.
39. Spray, D. C., A. L. Harris, and M. V. L. Bennett. 1981. Gap junctional conductance is a simple and sensitive function of intracellular pH. *Science (Wash. DC).* 211:712–715.
40. Stryer, L. 1981. Biochemistry, 2nd edition. W. H. Freeman and Company, San Francisco. 231.
41. Taylor, D. L., and J. S. Condeelis. 1979. Cytoplasmic structure and contractility in ameboid cells. *Int. Rev. Cytol.* 56:57–144.
42. Tsien, R., and R. Weingart. 1976. Inotropic effect of cyclic AMP in calf ventricular muscle studied by a cut-end method. *J. Physiol. (Lond.).* 260:117–141.
43. Van Holde, K. E. 1971. Physical Biochemistry. Prentice-Hall, Inc., Englewood Cliffs, New Jersey. 89.
44. Wang, Y. L., J. M. Heiple, and D. L. Taylor. 1982. Fluorescent analog cytochemistry of contractile proteins. *Methods Cell Biol.* 25:1–11.
45. Wang, Y. L., F. Lanni, P. L. McNeil, B. Ware, and D. L. Taylor. 1982. Mobility of cytoplasmic and membrane-associated actin in living cells. *Proc. Natl. Acad. Sci. USA.* 79:4660–4664.
46. Warner, A. E. 1979. Consequences of cell to cell signals in the early embryo. *In* The Role of Intercellular Signals: Navigation, Encounter, Outcome. J. G. Nicholls, editor. Verlag Chemie GMBH, Weinheim, Federal Republic of Germany. 179–200.
47. Warner, A. E., and P. Lawrence. 1982. Permeability of gap junctions at the segmental border in insect epidermis. *Cell.* 28:243–252.

48. Weidmann, S. 1966. The diffusion of radiopotassium across intercalated disks of mammalian cardiac muscle. *J. Physiol. (Lond.)*. 187:323–243.
49. Weingart, R. 1974. The permeability to tetraethylammonium ions of the surface membrane and intercalated disks of sheep and calf myocardium. *J. Physiol. (Lond.)*. 240:741–762.
50. Weir, M. P., and C. W. Lo. 1982. Gap junctional communication compartments in the Drosophila wing disk. *Proc. Natl. Acad. Sci. USA*. 79:3232–3235.
51. Willingham, M. C., and I. Pastan. 1978. The visualization of fluorescent proteins in living cells by video intensification microscopy. *Cell*. 13:501–507.
52. Wolpert, L. 1969. Positional information and the spatial pattern of cellular differentiation. *J. Theor. Biol*. 25:1–47.
53. Wolpert, L. 1978. Gap junctions: channels for communication in development. *In* Intercellular Junctions and Synapses. J. Feldman, N. B. Gilula, and J. D. Pitts, editors. Chapman & Hall, London. 83–96.